University of Kentucky
UKnowledge

Physics and Astronomy Faculty Publications

Physics and Astronomy

7-1-2015

Hard Three-Loop Corrections to Hyperfine Splitting in Positronium and Muonium

Michael I. Eides
University of Kentucky, eides@pa.uky.edu

Valery A. Shelyuto
D. I. Mendeleyev Institute for Metrology, Russia

Right click to open a feedback form in a new tab to let us know how this document benefits you.

Follow this and additional works at: https://uknowledge.uky.edu/physastron_facpub

Part of the Astrophysics and Astronomy Commons, and the Physics Commons

Hard Three-Loop Corrections to Hyperfine Splitting in Positronium and Muonium

Hard three-loop corrections to hyperfine splitting in positronium and muonium

Michael I. Eides[*]

Department of Physics and Astronomy, University of Kentucky, Lexington, Kentucky 40506, USA

Valery A. Shelyuto[†]

D. I. Mendeleyev Institute for Metrology, St. Petersburg 190005, Russia

We consider hard three-loop corrections to hyperfine splitting in muonium and positronium generated by the diagrams with closed electron loops. There are six gauge-invariant sets of such diagrams that generate corrections of order $m\alpha^7$. The contributions of these diagrams are calculated for an arbitrary electron-muon mass ratio without expansion in the small mass ratio. We obtain the formulas for contributions to hyperfine splitting that in the case of a small mass ratio describe corrections for muonium and in the case of equal masses describe corrections for positronium. The first few terms of the expansion of hard corrections in the small mass ratio were earlier calculated for muonium analytically. We check numerically that the new results coincide with the sum of the known terms of the expansion in the case of a small mass ratio. In the case of equal masses we obtain hard nonlogarithmic corrections of order $m\alpha^7$ to hyperfine splitting in positronium.

PACS numbers: 12.20.Ds, 31.30.jf, 32.10.Fn, 36.10.Dr

I. INTRODUCTION

For many years hyperfine splitting (HFS) in muonium and positronium has remained an active field of experimental and theoretical research. Results of highly accurate HFS measurements can be compared with the theoretical predictions of quantum electrodynamics obtained from the first principles without any adjustable parameters. Both experiment and theory have achieved very high accuracy. The experimental errors for HFS in muonium are now in the interval 16–51 Hz [1,2], and a new measurement with the goal to reduce the error to about 10 Hz or to a few parts in 10^9 is now planned at J-PARC [3,4]. The current theoretical uncertainty of HFS in muonium is about 70–100 Hz; see, e.g., reviews in Refs. [5–7]. Recent theoretical work on HFS in muonium concentrated on the calculation of radiative-recoil corrections of order $\alpha^3(m/M)E_F$ that arise from the three-loop diagrams with closed electron and muon loops [8–12]. The goal of this work is to reduce the theoretical error below 10 Hz.

The hyperfine splitting in positronium is measured with the error bars at the level of 1–2 MHz [13–16]. There is a discrepancy of about three standard deviations between the results of old and new experiments. A new measurement of the positronium HFS splitting is now planned at J-PARC [17]. All theoretical contributions to HFS in positronium of order $m\alpha^6$ and logarithmic corrections of order $m\alpha^7$ are already known; see, e.g., reviews in Refs. [18–20]. A new stage in the theory of positronium HFS was opened in Ref. [19] where the one-photon annihilation contribution of order $m\alpha^7$ was calculated. This paper was soon followed by the works of Adkins and collaborators [20,21], who calculated contributions of the light-by-light scattering insertion in the scattering and annihilation channels.

Hard nonlogarithmic contributions to HFS in positronium of order $m\alpha^7$ are similar to the radiative and radiative-recoil corrections to HFS in muonium of orders $\alpha^2(Z\alpha)E_F$ and $\alpha^2(Z\alpha)(m/M)E_F$, respectively. We calculated these corrections in muonium some time ago [8–12]. The corrections in muonium are power series in the electron-muon mass ratio with the coefficients enhanced by large logarithms of this mass ratio. The goal of the old work on muonium was to calculate the coefficients in this expansion, at least the factors before the logarithms, analytically. In the case of positronium the masses are equal and the hard corrections of order $m\alpha^7$ are pure numbers. We apply the approach developed for muonium to positronium. We consider an electromagnetically bound system of two particles with arbitrary masses M and m, and obtain general expressions for the hard corrections to HFS of order $m\alpha^7$ without expansion in the mass ratio of the constituents. We check numerically that in the case of a small mass ratio these formulas reproduce with high accuracy the sum of all already known terms in the expansion in the small mass ratio for muonium. We use the general expressions for the case of equal masses and calculate all hard three-loop contributions to HFS in positronium of order $m\alpha^7$ that are due to the diagrams with closed electron loops. The results

---
[*]Also at the Petersburg Nuclear Physics Institute, Gatchina, St. Petersburg 188300, Russia.
eides@pa.uky.edu, eides@thd.pnpi.spb.ru
[†]shelyuto@vniim.ru

of these calculations were reported in the rapid communication [22]. Below we present the details of the calculations in the general case of arbitrary mass ratio and in the special case of equal masses, for positronium.

II. CALCULATIONS

We start with the infrared-divergent contribution to HFS in muonium generated by the two-photon exchange diagrams in Fig. 1 calculated in the scattering approximation

$$
\Delta E = -\frac{Z\alpha}{\pi} E_F \frac{3mM}{16} \int \frac{d^4q}{i\pi^2 q^4} L^{\alpha\beta}_{e,\text{skel}}(q) L_{\mu,\text{skel},\alpha\beta}(-q)
$$
$$
= -\frac{Z\alpha}{\pi} E_F (2mM) \int \frac{d^4q}{i\pi^2 q^4} (2q^2 + q_0^2) L^{(e)}_{\text{skel}}(q) L^{(\mu)}_{\text{skel}}(-q),
$$
(1)

where

$$
L^{\alpha\beta}_{e,\text{skel}}(q) \equiv -\frac{2q^2}{q^4 - 4m^2 q_0^2} \gamma^\mu \hat{q} \gamma^\nu = 2L^{(e)}_{\text{skel}} \gamma^\mu \hat{q} \gamma^\nu
$$
(2)

FIG. 1. Diagrams with two-photon exchanges.

is the forward electron Compton scattering amplitude in the tree approximation (the skeleton electron-line factor), and $L^{\alpha\beta}_{\mu,\text{skel}}(q)$ is a similar amplitude for the muon. The Fermi energy is defined as $E_F = (8/3)(Z\alpha)^4 m_r^3/(mM)$, where $m_r = mM/(m+M)$ is the reduced mass. In the case of equal masses, $M = m$, the Fermi energy E_F turns into the leading nonannihilation contribution to HFS in positronium $E_F^{\text{Ps}} = m\alpha^4/3$. The external electron and muon lines in the diagrams in Fig. 1 are on the mass shell and carry zero spatial momenta. In the second line in Eq. (1) we calculated the projection of the matrix elements on HFS.

After the Wick rotation and transition to four-dimensional spherical coordinates ($q_0 = q\cos\theta$, $|\mathbf{q}| = q\sin\theta$) we obtain

$$
\Delta E = \frac{Z\alpha}{\pi} E_F \frac{4mM}{\pi} \int_0^\pi d\theta \sin^2\theta \int_0^\infty dq^2 (2 + \cos^2\theta) L^{(e)}_{\text{skel}} L^{(\mu)}_{\text{skel}}
$$
$$
= \frac{Z\alpha}{\pi} E_F \frac{4mM}{\pi} \int_0^\pi d\theta \sin^2\theta \int_0^\infty dq^2 \frac{2 + \cos^2\theta}{(q^2 + 4m^2\cos^2\theta)(q^2 + 4M^2\cos^2\theta)}
$$
$$
\equiv \frac{Z\alpha}{\pi} E_F \frac{mM}{M^2 - m^2} \int_0^\infty dq^2 f_\mu(q),
$$
(3)

where in the last step we rescaled the integration momentum $q \to qm$. The dimensionless weight function $f_\mu(q)$ in terms of an auxiliary function

$$
f(q) = -\frac{1}{4} + \frac{\sqrt{q^2+4}}{4q} - \frac{2\sqrt{q^2+4}}{q^3}
$$
(4)

has the form

$$
f_\mu(q) = f(q) - 4\mu^2 f(2\mu q),
$$
(5)

where $\mu = m/(2M)$.

In the case of positronium $M \to m$ and the weight function is simplified

$$
\frac{mM}{M^2 - m^2} f_\mu(q)\Big|_{M \to m} \to \frac{16 + 2q^2 + q^4 - q^3\sqrt{q^2+4}}{4q^3\sqrt{q^2+4}}
$$
$$
\equiv f_p(q).
$$
(6)

Respectively, the skeleton integral in Eq. (3) in the case of positronium turns into

$$
\Delta E = \frac{\alpha}{\pi} E_F^{\text{Ps}} \frac{4m^2}{\pi} \int_0^\pi d\theta \sin^2\theta \int_0^\infty dq^2 L^2_{e,\text{skel}} (2 + \cos^2\theta)
$$
$$
= \frac{\alpha}{\pi} E_F^{\text{Ps}} \frac{4m^2}{\pi} \int_0^\pi d\theta \sin^2\theta \int_0^\infty dq^2 \frac{2 + \cos^2\theta}{(q^2 + 4m^2\cos^2\theta)^2} \equiv \frac{\alpha}{\pi} E_F^{\text{Ps}} \int_0^\infty dq^2 f_p(q).
$$
(7)

The integrals in Eq. (3) and Eq. (7) are sums of an infrared linearly divergent integral and a finite one. In a more accurate approximation (with the off-mass-shell external fermion lines) the linear divergence is cut off at

the characteristic atomic scale $\lambda \sim m\alpha$ and generates an extra factor $m/\lambda \sim 1/\alpha$. As a result the infrared-divergent term turns into a contribution of order E_F that is of lower order in α. Therefore the uncertainty connected with the

lack of knowledge of the precise value of the infrared cutoff is hidden in the contribution to HFS that is of lower order in α and that anyway cannot be calculated in the scattering approximation. The remaining finite part of the integral originates at hard integration momenta $\sim m$ (or in the interval from m to M in the case of unequal masses) and generates a contribution of order αE_F. In the case of unequal masses, for muonium, the linearly infrared-divergent contribution turns into the leading nonrecoil Fermi contribution E_F to HFS, while the finite part generates the leading recoil correction of order $\alpha(m/M)E_F$; see, e.g., Refs. [5,6]. Let us emphasize that due to the linear (as opposed to logarithmic) nature of the apparent divergence it leaves no finite remnant of order αE_F and should be simply thrown away. No need in matching of high and low integration momenta arises. This feature should be contrasted with the case of a logarithmic infrared divergence when the cutoff at the atomic scale λ produces a logarithm $\ln(m/\lambda) \sim \ln(1/\alpha)$ and uncertainty in the precise value of the infrared cutoff generates uncontrolled nonlogarithmic contributions to HFS of the same order in α as the logarithmic term. This effect clearly indicates that an accurate matching of hard and soft momenta contributions is mandatory in the case of logarithmic infrared divergences. A rigorous formal proof of these features of linear and logarithmic infrared divergences can be found, e.g, in Refs. [23,24].

Six gauge-invariant sets of diagrams in Figs. 2–4 and in Figs. 6–8 generate hard radiative corrections of order $m\alpha^7$ that are due to the graphs with closed electron loops.[1] All these diagrams can be interpreted as the results of radiative insertions in the skeleton diagrams with two-photon exchanges in Fig. 1. It is well known that the insertion of radiative corrections suppresses the low-integration-momentum region; see, e.g., Refs. [5,6,23]. Hence, all diagrams in Figs. 2–4 and in Figs. 6–8 are infrared convergent.[2] Moreover, the characteristic integration momenta in these diagrams are hard (of order $\sim m$ or in the interval from m to M in the case of unequal masses) and are much larger than the atomic momenta of order $\sim m\alpha$, which justifies the validity of the scattering approximation for their calculation. This is exactly the approximation we used above in the calculation of the contribution of the skeleton diagrams in Fig. 1, and all corrections calculated below are obtained by some modifications of the basic integrals in Eq. (3) and Eq. (7).

A. Analytic results for one- and two-loop polarization insertions in the exchanged photons

Consider first the diagrams in Fig. 2 with two one-loop polarization loops. The insertion of a polarization operator

***

[1]All gauge-invariant sets of diagrams include the graphs with the crossed exchanged photons that we do not show explicitly.

[2]Linearly infrared-divergent contributions due to the anomalous magnetic moment should be subtracted from radiative corrections in Figs. 6 and 8; see more on this below.
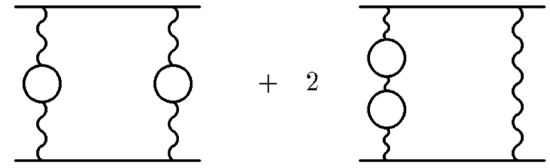

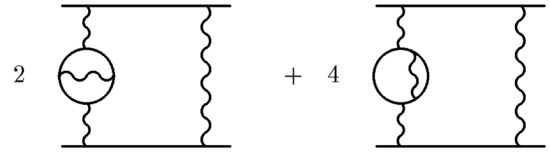FIG. 2. Diagrams with two one-loop polarization insertions.

FIG. 3. Diagrams with two-loop polarization insertions.

in a photon line with momentum q (all momenta below are measured in units of the electron mass) reduces to the replacement in the photon propagator

$$\frac{1}{q^2} \to \frac{\alpha}{\pi}I_1(q), \qquad (8)$$

where $(\alpha/\pi)I_1(q)$ is the well-known representation of the one-loop vacuum polarization [25].

$$\frac{\alpha}{\pi}I_1(q) = \frac{\alpha}{\pi}\int_0^1 dv \frac{v^2(1-\frac{v^2}{3})}{1-v^2}\frac{1}{q^2+\frac{4}{1-v^2}}. \qquad (9)$$

We see that a photon line that carries a polarization loop has a natural interpretation as a propagator of a massive photon with mass squared $\lambda^2 = 4/(1-v^2)$. According to Eq. (9) this propagator should be integrated over v with the weight $(\alpha/\pi)v^2(1-v^2/3)/(1-v^2)$.

The contribution of the diagrams in Fig. 2 is obtained by the insertion of the one-loop photon polarization squared $(\alpha/\pi)^2q^4I_1^2(q)$ in the integrands in Eq. (3) and Eq. (7). Due to the nonsingular behavior of the polarization operator at $q^2 \to 0$ we obtain convergent integrals where the effective integration momenta are hard, of order $\sim m$ (or in the interval from $\sim m$ to M in the case of unequal masses). Then in the general case of unequal masses the contribution to HFS has the form

$$\Delta E = 3\frac{\alpha^2(Z\alpha)}{\pi^3}E_F\frac{mM}{M^2-m^2}\int_0^\infty dq^2 f_\mu(q)q^4I_1^2(q), \quad (10)$$

where the factor 3 before the integral has a combinatorial origin. We checked numerically that in the small-mass-ratio limit this integral reproduces the sum of all analytically known terms [26,27] of the expansion of this contribution in the small mass ratio.

In the case of positronium the integral in Eq. (10) reduces to [compare Eq. (7)]
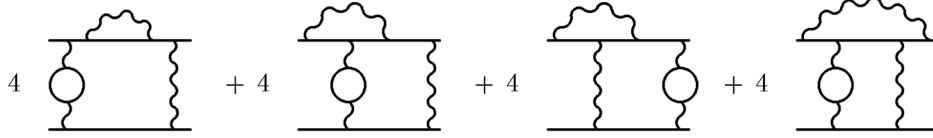
FIG. 4.   Diagrams with one-loop polarization and radiative photon insertions.

$$\Delta E_1 = 3\frac{\alpha^3}{\pi^3}E_F^{\mathrm{Ps}}\int_0^\infty dq^2 f_p(q)q^4 I_1^2(q), \qquad (11)$$

$$\Delta E_1 = \left(\frac{6\pi^2}{35}-\frac{8}{9}\right)\frac{\alpha^3}{\pi^3}E_F^{\mathrm{Ps}} = 0.803\,043\,294\frac{\alpha^3}{\pi^3}E_F^{\mathrm{Ps}}. \qquad (12)$$

and after computation we obtain the contribution to HFS of the diagrams with two one-loop polarization insertions in Fig. 2.

The contribution of the two-loop vacuum polarization in Fig. 3 can be obtained by the insertion of the two-loop photon polarization $(\alpha^2/\pi^2)q^2 I_2(q)$ [25,28] in the integrands in Eq. (3) and Eq. (7)

$$\left(\frac{\alpha}{\pi}\right)^2 I_2(q) = \frac{2}{3}\left(\frac{\alpha}{\pi}\right)^2\int_0^1 dv\frac{v}{4+q^2(1-v^2)}\left\{(3-v^2)(1+v^2)\left[\mathrm{Li}_2\left(-\frac{1-v}{1+v}\right)\right.\right.$$
$$\left.+2\mathrm{Li}_2\left(\frac{1-v}{1+v}\right)+\frac{3}{2}\ln\frac{1+v}{1-v}\ln\frac{1+v}{2}-\ln\frac{1+v}{1-v}\ln v\right]$$
$$+\left[\frac{11}{16}(3-v^2)(1+v^2)+\frac{v^4}{4}\right]\ln\frac{1+v}{1-v}$$
$$\left.+\left[\frac{3}{2}v(3-v^2)\ln\frac{1-v^2}{4}-2v(3-v^2)\ln v\right]+\frac{3}{8}v(5-3v^2)\right\}, \qquad (13)$$

where the dilogarithm is defined as $\mathrm{Li}_2(z) = -\int_0^1 dt\ln(1-zt)/t$.

In the case of unequal masses the integral for the contribution to HFS of the diagrams with the two-loop polarization in Fig. 3 has the form

$$\Delta E = 2\frac{\alpha^2(Z\alpha)}{\pi^3}E_F\frac{mM}{M^2-m^2}\int_0^\infty dq^2 f_\mu(q)q^2 I_2(q),$$
$$(14)$$

where the factor 2 before the integral is due to combinatorics. Again, due to the nonsingular behavior of the two-loop polarization at small $q^2 \to 0$ the integral in Eq. (14) is convergent, and typical integration momenta are hard, in the interval from m to M. We checked numerically that in the small-mass-ratio case the integral in Eq. (14) coincides with the sum of the known terms [26,27] of the expansion of this contribution to HFS in the small mass ratio.

In the case of equal masses, for positronium, the contribution to HFS of the diagrams in Fig. 3 reduces to the integral

$$\Delta E_2 = 2\frac{\alpha^3}{\pi^3}E_F^{\mathrm{Ps}}\int_0^\infty dq^2 f_p(q)q^2 I_2(q). \qquad (15)$$

This integral admits an analytic calculation, and we obtain

$$\Delta E_2 = \left[-\frac{217}{30}\zeta(3)+\frac{28\pi^2}{15}\ln 2+\frac{\pi^2}{675}+\frac{403}{360}\right]\frac{\alpha^3}{\pi^3}E_F^{\mathrm{Ps}}$$
$$= 5.209\,219\,614\frac{\alpha^3}{\pi^3}E_F^{\mathrm{Ps}}. \qquad (16)$$

B. One-loop electron factor and one-loop polarization insertion in the exchanged photon

The diagrams in Fig. 4 are obtained from the skeleton diagrams in Fig. 1 by one-loop radiative insertions in one of the exchanged photons and one of the fermion lines.[3] To describe these radiative insertions it is convenient to introduce the one-loop electron factor that is defined as a gauge-invariant sum of the diagrams in Fig. 5 where the external electron lines are on shell and carry zero spatial momenta (plus the diagrams with the exchanged external photon vertices). Physically the electron factor is a sum of one-loop corrections to the spin-dependent amplitude of the virtual forward Compton scattering.

The gauge-invariant electron factor $\tilde{L}_{\mu\nu}$ can be written as a sum of two gauge-invariant terms $\tilde{L}_{\mu\nu} = L_{\mu\nu} + L_{\mu\nu}^{(a)}$, where the term $L_{\mu\nu}^{(a)}$ is the contribution of the anomalous

---

[3]Multiplicity factors in these diagrams correspond to the case of positronium, not muonium.
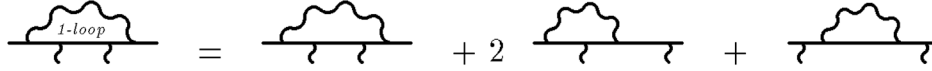
FIG. 5.   One-loop fermion factor.

magnetic moment (for more details see, e.g., Refs. [29,30]). The multiloop electron factors also can be written as sums of two gauge-invariant terms. The representation of the electron factor in the form of a sum of two gauge-invariant terms is convenient for calculations because these terms have different behavior at low virtual photon momenta. According to the generalized low-energy theorem (see, e.g., Refs. [5,6]) all terms linear in the small photon momentum q are due to the term $L_{\mu\nu}^{(a)}$, while the term $L_{\mu\nu}$ decreases at least as q^2 at small q^2. This different low-energy behavior

determines the structure of the integrals for the contributions to hyperfine splitting. In the case of the diagrams in Fig. 6 and in Fig. 8 the contributions to HFS generated by the term $L_{\mu\nu}^{(a)}$ are of lower order in α than the apparent order of a diagram. Technically the presence of the previous order contribution reveals itself as a linear infrared divergence of an integral calculated in the scattering approximation.

In the diagrams in Fig. 4 the skeleton fermion line in Fig. 1 is effectively replaced by the one-loop fermion factor $\tilde{L}_{\mu\nu}$ in Fig. 5, which can be described by the substitution

$$L_{e,\text{skel}}^{\mu\nu}(q) \to \tilde{L}^{\mu\nu}(q) = 2\frac{\alpha}{4\pi}\left\{\gamma^\mu\hat{q}\gamma^\nu\tilde{L}_{\text{I}}(q^2,q_0^2) + q_0\left[\gamma^\mu\gamma^\nu - \frac{q^\mu\hat{q}\gamma^\nu + \gamma^\mu\hat{q}q^\nu}{q^2}\right]\tilde{L}_{\text{II}}(q^2,q_0^2)\right\}, \tag{17}$$

where $\tilde{L}_{\text{I(II)}}$ are scalar form factors. The scalar form factors $\tilde{L}_{\text{I(II)}}$ have the form

$$\tilde{L}_{\text{I}} = L_{\text{I}} + L_A,$$
$$\tilde{L}_{\text{II}} = L_{\text{II}} - L_A, \tag{18}$$

where the scalar form factors $L_{\text{I(II)}}$ and L_A correspond to $L_{\mu\nu}$ and $L_{\mu\nu}^{(a)}$, respectively. The factor 2 before the brackets arises because we normalize the scalar form factors like the

skeleton one in Eq. (2), and the factor $\alpha/(4\pi)$ is due to the one-loop integration in the fermion factor.

The one-loop electron factor $L_{\mu\nu}$ with the subtracted contribution of the anomalous magnetic moment enters calculations of the two-loop radiative-recoil corrections to HFS in muonium, and we derived explicit integral representations for the respective scalar form factors $L_{\text{I(II)}}$ a long time ago [31–33]. After the Wick rotation, a rescaling of the integration momentum $q \to qm$, and the transition to the four-dimensional spherical coordinates the form factors can be written as

$$L_{\text{I}}(q^2,\cos^2\theta) = \int_0^1 dx \int_0^x dy \left\{ \frac{(q^2+a^2)[(q^2+a^2)^2 - 12b^2q^2\cos^2\theta]}{[(q^2+a^2)^2 + 4b^2q^2\cos^2\theta]^3}(c_1q^2\sin^2\theta + c_2q^4) \right.$$
$$\left. - \frac{(q^2+a^2)^2 - 4b^2q^2\cos^2\theta}{[(q^2+a^2)^2 + 4b^2q^2\cos^2\theta]^2}c_3q^2 + \frac{(q^2+a^2)4bq^2\cos^2\theta}{[(q^2+a^2)^2 + 4b^2q^2\cos^2\theta]^2}2c_4 \right\},$$

$$L_{\text{II}}(q^2,\cos^2\theta) = \int_0^1 dx \int_0^x dy \left\{ \frac{(q^2+a^2)4b}{[(q^2+a^2)^2 + 4b^2q^2\cos^2\theta]^2}c_5q^2 \right.$$
$$\left. - \frac{(q^2+a^2)^2 - 4b^2q^2\cos^2\theta}{[(q^2+a^2)^2 + 4b^2q^2\cos^2\theta]^2}2c_6q^2 + \frac{2b}{(q^2+a^2)^2 + 4b^2q^2\cos^2\theta}c_7q^2 \right\}, \tag{19}$$

where $a^2 = x^2/y(1-y)$, $b = (1-x)/(1-y)$, and the coefficient functions c_i are collected in Table I.

The scalar form factor L_A is proportional to the respective skeleton form factor L_{skel} in Eq. (2). After the Wick rotation and in terms of the dimensionless integration momentum q it has the form

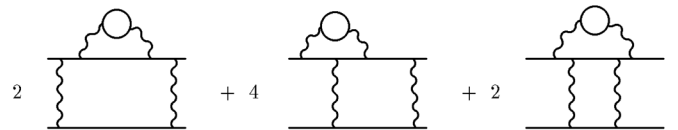$$L_A = \frac{2}{q^2 + 4\cos^2\theta} = 2L_{\text{skel}}. \tag{20}$$

FIG. 6.   Diagrams with one-loop polarization insertions in radiative photons.

TABLE I. Coefficients in the electron-line factor.

c_1	$\frac{16}{y(1-y)^3}[(1-x)(x-3y)-2y\ln x]$
c_2	$\frac{4}{y(1-y)^3}[-(1-x)(x-y-\frac{2y^2}{x})+2(x-4y+\frac{4y^2}{x})\ln x]$
c_3	$\frac{1}{y(1-y)^2}[1-6x-2x^2-\frac{y}{x}(26-\frac{6y}{x}-37x-2x^2+12xy$ $+16\ln x)]$
c_4	$\frac{1}{y(1-y)^2}(2x-4x^2-5y+7xy)$
c_5	$\frac{1}{y(1-y)^2}(6x-3x^2-8y+2xy)$
c_6	$-b^2\frac{x-y}{x^2}$
c_7	$2\frac{1-x}{x}$

In the case of unequal masses an analytic expression for the contribution to HFS of the diagrams in Fig. 4 is obtained by a modification of the skeleton integral in Eq. (3). First, we replace the skeleton factor in the integrand

$$(2+\cos^2\theta)L^{(e)}_{\text{skel}} \rightarrow \frac{\alpha}{4\pi}[(2+\cos^2\theta)\tilde{L}_\text{I}-3\cos^2\theta\tilde{L}_\text{II}].$$

(21)

The factor $\alpha/(4\pi)$ comes from the substitution in Eq. (17), and the term with $\tilde{L}_\text{II}$ arises because the one-loop electron factor in Eq. (17) contains an additional spinor structure in comparison with the skeleton one in Eq. (2).

Second, we need to account for the polarization loops in Fig. 4 and insert the term $2q^2I_1(q)$ into the integrand in Eq. (7). The factor 2 is due to the two ways of inserting the polarization operator into one of the exchanged photons. The polarization operator $q^2I_1(q)$ decreases like q^2 at small q, and we obtain an infrared convergent integral with hard characteristic integration momenta of order m (or in the interval from m to M in the case of unequal masses). Due to the suppression of the small integration momenta the anomalous magnetic moment in the diagrams in Fig. 4 gives a contribution on par with the other terms in the one-loop electron factor $\tilde{L}^{\mu\nu}(q)$.

Then the contribution to HFS of the diagrams in Fig. 4 in the case of unequal masses has the form

$$\Delta E = \frac{\alpha^2(Z\alpha)}{\pi^3}E_F\frac{M}{m}\frac{2}{\pi}\int_0^\infty dq^2 q^2 I_1(q)$$
$$\times \int_0^\pi d\theta\sin^2\theta L^{(\mu)}_{\text{skel}}[(2+\cos^2\theta)\tilde{L}_\text{I}-3\cos^2\theta\tilde{L}_\text{II}].$$

(22)

The leading terms of the expansion of the contribution to HFS in Eq. (22) in the small mass ratio have been known for some time [26,33,34].

$$\Delta E = \frac{\alpha^2(Z\alpha)}{\pi^3}E_F\left[\pi^2\left(-\frac{4}{3}\ln^2\frac{1+\sqrt{5}}{2}-\frac{20}{9}\sqrt{5}\ln\frac{1+\sqrt{5}}{2}-\frac{64}{45}\ln 2+\frac{\pi^2}{9}+\frac{3}{8}+\frac{1043}{675}\right)\right.$$
$$\left.+\frac{m}{M}\left(\frac{5}{2}\ln^2\frac{M}{m}+\frac{10}{3}\ln\frac{M}{m}+11.41788\right)\right].$$

(23)

We have checked numerically that the integral in Eq. (22) coincides with this analytical result in the case of a small mass ratio.

In the case of equal masses there is an extra factor 2 before the diagrams in Fig. 4. This factor arises because now there are two ways to insert the fermion factor into one of the lepton lines. Hence, the respective contribution to HFS is described by the double integral in Eq. (22) at $M=m$. Then we obtain the contribution of the diagrams in Fig. 4 to HFS in positronium in the form

$$\Delta E_3 = \frac{\alpha^3}{\pi^3}E^\text{Ps}_F\frac{4}{\pi}\int_0^\infty dq^2 q^2 I_1(q)$$
$$\times \int_0^\pi d\theta\sin^2\theta L_{\text{skel}}[(2+\cos^2\theta)\tilde{L}_\text{I}-3\cos^2\theta\tilde{L}_\text{II}]$$
$$= -1.28709\,(1)\frac{\alpha^3}{\pi^3}E^\text{Ps}_F.$$

(24)

C. One-loop polarization insertion in the electron factor

Consider now the diagrams in Fig. 6 with the one-loop polarization insertions in the radiative photon.[4] Effectively these diagrams contain a massive radiative photon; see Eq. (8) and Eq. (9). In principle, the respective electron factor can be obtained from the one-loop electron factor in Eq. (17) by restoring the radiative photon mass squared $\lambda^2 = 4m^2/(1-v^2)$, followed by integration over v with the weight $(\alpha/\pi)v^2(1-v^2/3)/(1-v^2)$. However, the relatively compact expression in Eq. (17) is a result of numerous cancellations in the integrand between the contributions from different diagrams in Fig. 5, and technically it is much easier to start the calculation of the two-loop electron factor in Fig. 6 from scratch. We consider this electron factor as a sum of the

---

[4]Multiplicity factors in these diagrams correspond to the case of positronium, not muonium.

contributions corresponding to the separate diagrams in Fig. 6 with the self-energy, vertex and spanning photon insertions in the electron line. Each of these terms is calculated as a one-loop diagram with a massive photon and then integrated over the auxiliary parameter v as we just explained.

The only subtlety in further calculations is connected with the diagrams with the vertex correction in Fig. 6. All entries in the two-loop fermion factor except the two-loop anomalous magnetic moment carry at least one extra power of q^2 at $q^2 \to 0$ in comparison with the skeleton electron factor. One can separate the contribution to the two-loop anomalous magnetic moment from the two-loop vertex in the second diagram in Fig. 6 in a gauge-invariant way, like we separated the one-loop anomalous magnetic moment from the one-loop electron factor $L_{\mu\nu}$ above. The two-loop anomalous magnetic moment term in the second diagram in Fig. 6 generates a linearly infrared-divergent contribution to HFS. This linear infrared divergence that is cut off at the characteristic atomic scale $\sim m\alpha$ indicates that the anomalous magnetic moment generates a contribution to HFS of the previous order in α. This correction of order $m\alpha^6$ was already accounted for in earlier calculations and we should simply delete the apparently divergent term that generates it. To get rid of the spurious divergence we subtract the gauge-invariant term with the two-loop anomalous magnetic moment from the two-loop electron vertex in Fig. 6. The subtracted two-loop electron factor in Fig. 6 can be written in terms of scalar two-loop form factors $L_{\mathrm{I,II}}^{(2)}$

$$L_{\mathrm{I,II}}^{(2)} = L_{\mathrm{I,II}}^{(2,\Sigma)} + 2L_{\mathrm{I,II}}^{(2,\Lambda)} + L_{\mathrm{I,II}}^{(2,\Xi)} \tag{25}$$

similar to the one-loop form factors $L_{\mathrm{I,II}}$ in Eq. (18). Unlike the one-loop form factors $\tilde{L}_{\mathrm{I,II}}$ in Eq. (17) these two-loop form factors do not include contributions of the anomalous magnetic moment.

In terms of the scalar form factors in Eq. (25) the contribution to HFS of the diagrams in Fig. 6 in the general case has the form

$$\Delta E = \frac{\alpha^2(Z\alpha)}{\pi^3} E_F \frac{M}{m} \frac{1}{\pi} \int_0^\infty dq^2$$
$$\times \int_0^\pi d\theta \sin^2\theta L_{\mathrm{skel}}^{(\mu)} \left[(2 + \cos^2\theta)L_{\mathrm{I}}^{(2)} - 3\cos^2\theta L_{\mathrm{II}}^{(2)} \right]. \tag{26}$$

We have derived and used explicit expressions for the two-loop form factor in Eq. (25) in Refs. [10,35], where we calculated the nonrecoil and radiative-recoil corrections to HFS in muonium due to the diagrams in Fig. 6. Explicit expressions for the contributions to the energy shifts in Eqs. (2), (26) and (31) from Ref. [10] correspond to the integral in Eq. (26) with the three terms on the rhs in Eq. (25) and were obtained without expansion in the small

mass ratio. They are rather cumbersome and we will not reproduce them here. Using these expressions we obtain a few leading terms of the expansion in the small mass ratio of the contribution of the diagrams in Fig. 6 to HFS that were calculated earlier

$$\Delta E = \frac{\alpha^2(Z\alpha)}{\pi^3} E_F \Big\{ -0.310742\pi^2$$
$$+ \frac{m}{M} \left[\frac{3}{4} \ln^2 \frac{M}{m} + \left(\pi^2 - \frac{53}{6} \right) \ln \frac{M}{m} + 7.08072 \right] \Big\}. \tag{27}$$

We have checked numerically that the expression in Eq. (26) derived for arbitrary masses reproduces the expansion above in the case of a small mass ratio.

In the case of equal masses the contribution of the diagrams in Fig. 6 to HFS reduces to

$$\Delta E_4 = \frac{\alpha^3}{\pi^3} E_F^{\mathrm{Ps}} \frac{2}{\pi} \int_0^\infty dq^2 \int_0^\pi d\theta \sin^2\theta L_{\mathrm{skel}}$$
$$\times [(2 + \cos^2\theta)L_{\mathrm{I}}^{(2)} - 3\cos^2\theta L_{\mathrm{II}}^{(2)}], \tag{28}$$

where an extra factor 2 before the integral [in comparison with Eq. (26)] arises because we can insert the two-loop electron factor into either of the fermion lines.

After calculations we obtain

$$\Delta E_4 = -3.15441(1) \frac{\alpha^3}{\pi^3} E_F^{\mathrm{Ps}}. \tag{29}$$

D. Light-by-light scattering contribution

Due to gauge invariance the light-by-light scattering block decreases fast with the momenta of the external (virtual) photons. Therefore, effectively all integration momenta in the diagrams in Fig. 7 are hard, of order of the electron mass (or in the interval from m to M in the case of unequal masses).

The contribution of the light-by-light scattering block to HFS in the general case of unequal masses has the form [12,30].

$$\Delta E = \frac{\alpha^2(Z\alpha)}{\pi^3} E_F \frac{3M^2}{32\pi} \int_0^\infty \frac{dq^2}{q^2}$$
$$\times \int_0^\pi d\theta \sin^2\theta \frac{T(q^2, \cos^2\theta)}{m^2 q^2 + 4M^2 \cos^2\theta}. \tag{30}$$
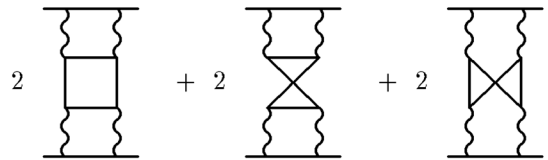

FIG. 7.   Diagrams with light-by-light scattering insertions.

The explicit integral representation for the function $T(q^2, \cos^2\theta)$ and its definition in terms of the light-by-light scattering tensor can be found in Refs. [11,12]. We use in Eq. (30) four-dimensional spherical coordinates introduced above Eq. (3), so q_0 from Ref. [12] becomes $q\cos\theta$.

The first terms of the expansion of this contribution to HFS in the small mass ratio were calculated during many years [11,12,36,37].

$$\Delta E = \frac{\alpha^2(Z\alpha)}{\pi^3} E_F \left\{ -0.472\,514(1)\pi^2 \right.$$
$$+ \frac{m}{M}\left[\frac{9}{4}\ln^2\frac{M}{m} + \left(-3\zeta(3) - \frac{2\pi^2}{3} + \frac{91}{8}\right)\ln\frac{M}{m} \right.$$
$$\left.\left. + 5.9949(1)\right]\right\}. \tag{31}$$

We have checked numerically that the general expression in Eq. (30) coincides with the sum in Eq. (31) in the case of a small mass ratio.

In the case of equal masses the integral in Eq. (30) reduces to[5]

$$\Delta E_5 = \frac{\alpha^3}{\pi^3} E_F^{\mathrm{Ps}} \frac{3}{32\pi} \int_0^\infty \frac{dq^2}{q^2} \int_0^\pi d\theta \sin^2\theta \frac{T(q^2, \cos^2\theta)}{q^2 + 4\cos^2\theta}. \tag{32}$$

The calculation of this contribution to HFS in positronium proceeds exactly like the calculation of the respective nonlogarithmic radiative-recoil correction to HFS in muonium in Ref. [12] and we obtain

$$\Delta E_5 = -0.706\,27(5)\frac{\alpha^3}{\pi^3} E_F^{\mathrm{Ps}}, \tag{33}$$

which coincides with the result first obtained in Ref. [20].

E. Two one-loop electron factors

The diagrams in Fig. 8 contain the one-loop fermion factors from Eq. (17) in both fermion lines. Naively, the contribution of these diagrams to HFS can be obtained from the skeleton integral in Eq. (3) by the replacement

$$L_{\mathrm{skel}}^{(e)} L_{\mathrm{skel}}^{(\mu)}(2 + \cos^2\theta) \to \left(\frac{\alpha}{4\pi}\right)^2 [(2 + \cos^2\theta)\tilde{L}_{\mathrm{I}}^{(e)}\tilde{L}_{\mathrm{I}}^{(\mu)} - 3\cos^2\theta(\tilde{L}_{\mathrm{I}}^{(e)}\tilde{L}_{\mathrm{II}}^{(\mu)} + \tilde{L}_{\mathrm{II}}^{(e)}\tilde{L}_{\mathrm{I}}^{(\mu)}) + \cos^2\theta(1 + 2\cos^2\theta)\tilde{L}_{\mathrm{II}}^{(e)}\tilde{L}_{\mathrm{II}}^{(\mu)}], \tag{34}$$

where the terms on the right-hand side arise after the calculation of the projection of the product of two electron factors [see Eq. (17)] on the HFS structure.

The scalar form factors $\tilde{L}_{\mathrm{I,II}}^{(e,\mu)}$ include terms with the scalar form factors $L_A^{(e,\mu)}$ arising due to anomalous magnetic moments; see Eq. (18). Therefore, each product of the scalar functions in the square brackets on the right-hand side of Eq. (34) contains the term $L_A^{(e)}L_A^{(\mu)}$. As we already mentioned the form factors $L_{\mathrm{I,II}}^{(e,\mu)}$ decrease at least as q^2 at $q^2 \to 0$ relative to the skeleton form factors, while the form factors $L_A^{(e,\mu)}$ behave exactly like the skeleton form factors; see Eq. (20). Hence, each integral of $L_A^{(e)}L_A^{(\mu)}$ is a sum of a linearly infrared-divergent and finite contributions, compare with the skeleton integral in Eq. (3). In a more accurate calculation the linearly infrared-divergent contribution would be cut off at the atomic scale $\sim m\alpha$ and would generate a correction of lower order in α. It should be simply subtracted, while we need to preserve the finite part of the integral that generates a correction of order $m\alpha^7$. In the general case of different masses (for example, for muonium) the finite part is a recoil contribution and it was calculated in

Ref. [29]. It is equal to $(9/16)(mM)/(M^2 - m^2)\ln(M^2/m^2)$ up to a normalization factor. Hence, the subtraction of the linearly infrared-divergent contribution due to terms with $L_A^{(e)}L_A^{(\mu)}$ in Eq. (34) reduces to the addition of $(9/16)(mM)/(M^2 - m^2)\ln(M^2/m^2)$ to the respective contribution to HFS instead of all of the terms on the right-hand side in Eq. (34) that are proportional to $L_A^{(e)}L_A^{(\mu)}$. After this replacement of the infrared-divergent part we obtain a convergent integral with hard characteristic integration momenta in the interval from m to M. The contribution to HFS of the diagrams in Fig. 8 in the case of unequal masses has the form
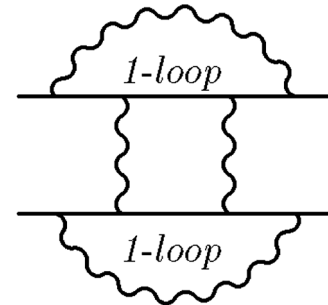

FIG. 8. Diagrams with one-loop radiative photon insertions in both fermion lines.

---

[5]There is a misprint in the respective expression in Eq. (14) in Ref. [22].

$$\Delta E = \frac{\alpha(Z^2\alpha)(Z\alpha)}{\pi^3} E_F \left\{ \frac{M}{m} \frac{1}{4\pi} \int_0^\infty dq^2 \int_0^\pi d\theta \sin^2\theta d\theta [(2+\cos^2\theta)(L_I^{(e)}L_I^{(\mu)} + L_A^{(e)}L_I^{(\mu)} + L_A^{(\mu)}L_I^{(e)}) \right.$$

$$- 3\cos^2\theta(L_I^{(e)}L_{II}^{(\mu)} + L_A^{(e)}L_{II}^{(\mu)} - L_I^{(e)}L_A^{(\mu)} + L_{II}^{(e)}L_I^{(\mu)} - L_A^{(e)}L_I^{(\mu)} + L_{II}^{(e)}L_A^{(\mu)})$$

$$\left. + \cos^2\theta(1+2\cos^2\theta)(L_{II}^{(e)}L_I^{(\mu)} - L_A^{(e)}L_{II}^{(\mu)} - L_{II}^{(e)}L_A^{(\mu)})] + \frac{9}{16}\frac{mM}{M^2-m^2}\ln\frac{M^2}{m^2} \right\}. \tag{35}$$

The first terms of the expansion of the contribution to HFS of the diagrams in Fig. 8 in the small mass ratio have been known for some time [29,38].

$$\Delta E = \frac{\alpha(Z^2\alpha)(Z\alpha)}{\pi^3} E_F \left[\frac{\pi^2}{2}\left(\ln 2 - \frac{13}{4}\right) \right.$$

$$+ \frac{m}{M}\left(-\frac{9}{8}\ln\frac{M}{m} - \frac{15}{8}\zeta(3) + \frac{15\pi^2}{4}\ln 2 + \frac{37\pi^2}{24} - \frac{147}{32}\right)$$

$$\left. + \frac{9}{16}\frac{Mm}{M^2-m^2}\ln\frac{M^2}{m^2} \right]. \tag{36}$$

We have checked numerically that in the case of a small mass ratio the expression in Eq. (35) coincides with the sum above.

In the case of equal masses the integral in Eq. (35) is simplified

$$\Delta E_6 = \frac{\alpha^3}{\pi^3} E_F^{Ps} \left\{ \frac{1}{4\pi} \int_0^\infty dq^2 \int_0^\pi d\theta \sin^2\theta d\theta [(2+\cos^2\theta) \right.$$

$$\times (L_I^2 + 2L_A L_I) - 6\cos^2\theta(L_I L_{II} + L_A L_{II} - L_A L_I)$$

$$\left. + \cos^2\theta(1+2\cos^2\theta)(L_{II}^2 - 2L_A L_{II})] + \frac{9}{16} \right\}. \tag{37}$$

After numerical calculations we obtain the contribution of the diagrams in Fig. 8 to HFS in positronium

$$\Delta E_6 = -4.739\,55\,(40)\frac{\alpha^3}{\pi^3} E_F^{Ps}. \tag{38}$$

III. SUMMARY OF RESULTS

We have derived explicit expressions for hard three-loop contributions to hyperfine splitting generated by the six gauge-invariant sets of diagrams with closed electron loops in Figs. 2–4 and in Figs. 6–8. In the case of unequal lepton masses we confirmed numerically the already known

results for muonium obtained earlier in the form of an expansion in the small mass ratio. We have calculated the contributions of these diagrams to HFS in the case of equal masses, for positronium. Collecting the results in Eqs. (12), (16), (24), (29), (33), and (38), we obtain the total hard contribution to HFS in positronium of order $m\alpha^7$ generated by all diagrams with closed electron loops in Figs. 2–4 and in Figs. 6–8.

$$\Delta E = -3.875\,0\,(4)\left(\frac{\alpha}{\pi}\right)^3 E_F^{Ps} = -1.291\,7\,(1)\frac{m\alpha^7}{\pi^3}$$

$$= -5.672 \text{ kHz}. \tag{39}$$

Taking into account all other recent theoretical results [19–21] we obtain the theoretical prediction for HFS in positronium

$$\Delta E_{theor} = 203\,391.89\,(25) \text{ MHz}. \tag{40}$$

The latest experimental result is [16].

$$\Delta E_{exp} = 203\,394.2\,(1.6)_{stat}\,(1.3)_{sys} \text{ MHz}. \tag{41}$$

There are no contradictions between theory and experiment at the present level of accuracy, but further reduction of both the experimental and theoretical uncertainties is warranted. The calculation of the remaining ultrasoft and hard nonlogarithmic contributions of order $m\alpha^7$ is the next task for the theory. We hope to report the results for the remaining hard corrections in the near future.

[1] F. G. Mariam *et al.*, Phys. Rev. Lett. **49**, 993 (1982).

[2] W. Liu *et al.*, Phys. Rev. Lett. **82**, 711 (1999).

[3] Ken-ichi Sasaki, M. Sugano, H. Iinuma, T. Ogitsu, N. Saito, K. Shimomura, and A. Yamamoto, J. Phys. Conf. Ser. **408**, 012074 (2013).

[4] K. S. Tanaka *et al.*, J. Phys. Soc. Jpn. Conf. Proc. **2**, 010405 (2014).

[5] M. I. Eides, H. Grotch, and V. A. Shelyuto, Phys. Rep. **342**, 63 (2001).

[6] M. I. Eides, H. Grotch, and V. A. Shelyuto, *Theory of Light Hydrogenic Bound States*, (Springer, New York, 2007).

[7] P. J. Mohr, B. N. Taylor, and D. B. Newell, Rev. Mod. Phys. **84**, 1527 (2012).

[8] M. I. Eides and V. A. Shelyuto, Phys. Rev. Lett. **103**, 133003 (2009).

[9] M. I. Eides and V. A. Shelyuto, Phys. Rev. D **80**, 053008 (2009).

[10] M. I. Eides and V. A. Shelyuto, Zh. Eksp. Teor. Fiz. **137**, 24 (2010) [J. Exp. Theor. Phys. **110**, 17 (2010)].

[11] M. I. Eides and V. A. Shelyuto, Phys. Rev. D **87**, 013005 (2013).

[12] M. I. Eides and V. A. Shelyuto, Phys. Rev. D **89**, 014034 (2014).

[13] A. P. Mills, Jr. and G. H. Bearman, Phys. Rev. Lett. **34**, 246 (1975).

[14] M. W. Ritter, P. O. Egan, V. W. Hughes, and K. A. Woodle, Phys. Rev. A **30**, 1331 (1984).

[15] A. P. Mills, Phys. Rev. A **27**, 262 (1983).

[16] A. Ishida, T. Namba, S. Asai, T. Kobayashi, H. Saito, M. Yoshida, K. Tanaka, and A. Yamamoto, Phys. Lett. B **734**, 338 (2014).

[17] A. Ishida, in *Proceedings of the Fundamental Constants Meeting, Eltville, Germany, February 1–6, 2015* (to be published).

[18] A. A. Penin, *Proc. Sci.*, LL2014 (2014) 074.

[19] M. Baker, P. Marquard, A. A. Penin, J. Piclum, and M. Steinhauser, Phys. Rev. Lett. **112**, 120407 (2014).

[20] G. S. Adkins and R. N. Fell, Phys. Rev. A **89**, 052518 (2014).

[21] G. S. Adkins, C. Parsons, M. D. Salinger, R. Wang, and R. N. Fell, Phys. Rev. A **90**, 042502 (2014).

[22] M. I. Eides and V. A. Shelyuto, Phys. Rev. D **89**, 111301(R) (2014).

[23] M. I. Eides, S. G. Karshenboim, and V. A. Shelyuto, Ann. Phys. (Amsterdam) **205**, 231 (1991).

[24] J. R. Sapirstein, E. A. Terray, and D. R. Yennie, Phys. Rev. D **29**, 2290 (1984).

[25] J. Schwinger, *Particles, Sources and Fields, Vol. 2* (Addison-Wesley, Reading, MA, 1973).

[26] M. I. Eides, S. G. Karshenboim, and V. A. Shelyuto, Pis'ma Zh. Eksp. Teor. Fiz. **50**, 3 (1989) [Phys. Lett. B **229**, 285 (1989)]; Yad. Fiz. **50**, 1636 (1989) [JETP Lett. **50**, 1 (1989)]; [Sov. J. Nucl. Phys. **50**, 1015 (1989)].

[27] M. I. Eides, H. Grotch, and V. A. Shelyuto, Phys. Rev. D **65**, 013003 (2001).

[28] G. Kallen and A. Sabry, K. Dan. Vidensk. Selsk. Mat. Fys. Medd. **29**, 17 (1955).

[29] M. I. Eides, H. Grotch, and V. A. Shelyuto, Phys. Rev. D **70**, 073005 (2004); **88**, 119901(E) (2013).

[30] M. I. Eides and V. A. Shelyuto, Phys. Rev. D **90**, 113002 (2014).

[31] V. Yu. Brook, M. I. Eides, S. G. Karshenboim, and V. A. Shelyuto, Phys. Lett. B **216**, 401 (1989).

[32] M. I. Eides, H. Grotch, and V. A. Shelyuto, Phys. Rev. D **58**, 013008 (1998).

[33] M. I. Eides, H. Grotch, and V. A. Shelyuto, Phys. Rev. D **67**, 113003 (2003).

[34] M. I. Eides, H. Grotch, and V. A. Shelyuto, Can. J. Phys. **83**, 363 (2005).

[35] M. I. Eides, S. G. Karshenboim, and V. A. Shelyuto, Phys. Lett. B **249**, 519 (1990); Pis'ma Zh. Eksp. Teor. Fiz. **52**, 937 (1990) [JETP Lett. **52**, 317 (1990)].

[36] M. I. Eides, S. G. Karshenboim, and V. A. Shelyuto, Phys. Lett. B **268**, 433 (1991); **316**, 631(E) (1993); Yad. Fiz. **55**, 466 (1992); Phys. Lett. B **319**, 545(E) (1993); Sov. J. Nucl. Phys. **55**, 257 (1992); Yad. Fiz. **57**, 1343(E) (1994) [Sov. J. Nucl. Phys. **57**, 1275(E) (1994)].

[37] M. I. Eides, S. G. Karshenboim, and V. A. Shelyuto, Phys. Lett. B **216**, 405 (1989); Yad. Fiz. **49**, 493 (1989) [Sov. J. Nucl. Phys. **49**, 309 (1989)].

[38] N. Kroll and F. Pollock, Phys. Rev. **84**, 594 (1951); **86**, 876 (1952).